Chemistry–A European Journal
Research Article
doi.org/10.1002/chem.202401033
Chemistry Europe
European Chemical Societies Publishing
www.chemeurj.org

Hot Paper

U(V) Stabilization via Aliovalent Incorporation of Ln(III) into Oxo-salt Framework

Yi Yu[+],[a] Yucheng Hao[+],*[b] Bin Xiao,[c] Eike Langer,[c] Sergei A. Novikov,[d] Harry Ramanantoanina,[e] Ivan Pidchenko,[e] Dieter Schild,[e] Thomas E. Albrecht-Schoenzart,[f] Rüdiger-A. Eichel,[g] Tonya Vitova,[e] and Evgeny V. Alekseev*[g]

Pentavalent uranium compounds are key components of uranium's redox chemistry and play important roles in environmental transport. Despite this, well-characterized U(V) compounds are scarce primarily because of their instability with respect to disproportionation to U(IV) and U(VI). In this work, we provide an alternate route to incorporation of U(V) into a crystalline lattice where different oxidation states of uranium can be stabilized through the incorporation of secondary cations with different sizes and charges. We show that iriginite-based crystalline layers allow for systematically replacing U(VI) with U(V) through aliovalent substitution of 2+ alkaline-earth or 3+ rare-earth cations as dopant ions under high-temperature conditions, specifically $Ca(U^{VI}O_2)W_4O_{14}$ and $Ln(U^{V}O_2)W_4O_{14}$ (Ln = Nd, Sm, Eu, Gd, Yb). Evidence for the existence of U(V) and U(VI) is supported by single-crystal X-ray diffraction, high energy resolution X-ray absorption near edge structure, X-ray photoelectron spectroscopy, and optical absorption spectroscopy. In contrast with other reported U(V) materials, the U(V) single crystals obtained using this route are relatively large (several centimeters) and easily reproducible, and thus provide a substantial improvement in the facile synthesis and stabilization of U(V).

Introduction

Actinides show a great diversity in their chemistries due to the complex structure of 5*f* electron shells.[1–6] One of the remarkable properties of actinides is the multivalence which has a very strong influence on their chemical and physical properties. Uranium is an important element from the actinides series and it is widely used for energy production. Uranium compounds have been isolated in oxidation states from II to VI in solid state with IV and VI being the most common.[7–9] Pentavalent uranium, U(V), which possesses a single 5*f* electron, represents the simplest configuration of f-electrons.[10,11] U(V) complexes are notable for their role as substitutes for the more radioactive neptunyl ion $[Np(V)O_2]^+$, a crucial element in nuclear waste.[12,13] Studying the physical and chemical properties of U(V) is vital for better understanding uranium's environmental effects,[14] its handling in waste disposal,[15] and the treatment of spent nuclear fuel.[16] This form of uranium is also instrumental in simplifying theoretical models and deepening our knowledge of f-electron behavior in actinides.[17–20] Although U(V) holds substantial environmental and fundamental value, report on U(V) remains rare because of its tendency to undergo disproportionation, leading to reactivity with air and water.[21] Finding facile techniques to stabilize materials containing pentavalent uranium are still a considerable challenge. In this work, we present a novel approach to modulate the oxidation state of uranium by incorporating cations of varying sizes and charges into a complex system. We show the hexavalent uranium U(VI) and pentavalent uranium U(V) can be stabilized in the isostructural compounds of alkaline-earth metal-based $Ca(U^{VI}O_2)W_4O_{14}$ and lanthanide-based $[Ln(U^{V}O_2)W_4O_{14}]$ (Ln = Nd, Sm, Eu, Gd, and Yb), respectively. The detailed crystal structures, proposed charge-compensating mechanism and spectroscopic investigations of these compounds were performed in respect

[a] *Y. Yu*[+]
School of Physics and Electronics information, Gannan Normal University, Ganzhou 341000, PR China
[b] *Y. Hao*[+]
School of Energy Materials and Chemical Engineering, Hefei University, Hefei, 230000, PR China
[c] *B. Xiao, E. Langer*
Institute of Energy and Climate Research (IEK-6), Forschungszentrum Jülich, D-52428 Jülich, Germany
[d] *S. A. Novikov*
Department of Chemistry, University of Georgia 302 East Campus Road, Athens, GA 30602, USA
[e] *H. Ramanantoanina, I. Pidchenko, D. Schild, T. Vitova*
Institute for Nuclear Waste Disposal (INE), Karlsruhe Institute of Technology, D-76125 Karlsruhe, Germany
g
[f] *T. E. Albrecht-Schoenzart*
Department of Chemistry and Nuclear Science and Engineering Center, Colorado School of Mines, Golden, Colorado, 80401 USA
[g] *R.-A. Eichel, E. V. Alekseev*
Institute of Energy and Climate Research (IEK-9), Forschungszentrum Jülich, D-52428 Jülich, Germany,
E-mail: e.alekseev@fz-juelich.de
haoyco@hfuu.edu.cn
[+] *These authors contributed equally to this work.*

Supporting information for this article is available on the WWW under https://doi.org/10.1002/chem.202401033

to uranium valence state and to an influence of lanthanide cations on U(V) stabilization within the oxo-framework.

Results and Discussion

$Ca(U^{VI}O_2)W_4O_{14}$ and $Ln(U^{V}O_2)W_4O_{14}$ (Ln = Nd, Sm, Eu, Gd, and Yb) series were synthesized via high-temperature solid-state reaction under air atmosphere condition, and formed as high-quality large crystals. To the best of our knowledge, $Ln(U^{V}O_2)W_4O_{14}$ series are the first oxo-salt materials containing both pentavalent uranium and rare-earth metals to be structurally characterized through single crystal diffraction. It is also the first example of a U(V) compound in which the apical O atoms of the uranyl unit interact directly with rare-earth polyhedra (U–Ln cation-cation interaction, highlighted in Figure 1). Single crystal XRD analysis reveals that $Ca(U^{VI}O_2)W_4O_{14}$ and $Ln(U^{V}O_2)W_4O_{14}$ are isostructural. Both compounds crystallize with the monoclinic space group with two crystallographically independent W atoms, one U atom and one Ln or Ca atom in an asymmetric unit (see Figure 1 (a)). They form a condensed

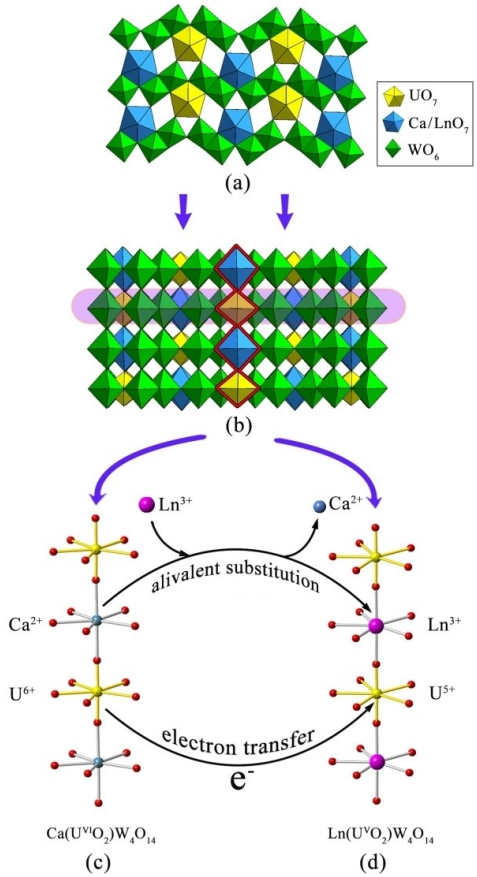

Figure 1. (a) The polyhedral presentation of the three-dimensional framework in the isostructural $Ln(U^{V}O_2)W_4O_{14}$ and $Ca(U^{VI}O_2)W_4O_{14}$ compounds. Legends: The green and yellow colors are WO_6 and UO_7 polyhedra, respectively. The blue color is CaO_7 or LnO_7 in $Ca(U^{VI}O_2)W_4O_{14}$ or $Ln(U^{V}O_2)W_4O_{14}$. (b) The framework can be subdivided into iriginite-type layers. (c, d) Representation of the charge-compensation mechanism when Ca^{2+} ions are substituted in the host phase of $Ca(U^{VI}O_2)W_4O_{14}$ with Ln^{3+} ions to result in $Ln(U^{V}O_2)W_4O_{14}$.

three-dimensional (3D) framework that can be reasonably separated into iriginite-type layers.[22–25] Part of the layers in $Ln(U^{V}O_2)W_4O_{14}$ and $Ca(U^{VI}O_2)W_4O_{14}$ are shown in Figure 1 (b). It is important to note that the iriginite-type layers are also commonly observed for a number of minerals and synthetic inorganic compounds.[7–9] Within the layer, edge-sharing $[W_2O_{10}]$ dimers are connected by sharing corners, creating tungsten-oxygen chains that are one polyhedron wide. Adjacent tungsten chains are fused into the layer by bridging UO_7 pentagonal bipyramids. The resulting layers are stacked perpendicular to the layer plane by sharing apical O atoms of WO_6 octahedra, resulting in the 3D anionic U–W–O framework with infinite corrugated $[W_4O_{11}]^{2+}$ tungsten slabs in the direction normal to the plane of the layer. As shown in Figure 1 (a, b), the cavities within each U–W–O anionic framework are filled by the seven-fold coordinated LnO_7 and CaO_7 polyhedra in $Ln(U^{V}O_2)W_4O_{14}$ and $Ca(U^{VI}O_2)W_4O_{14}$, respectively. Although the $Ln(U^{V}O_2)W_4O_{14}$ and $Ca(U^{VI}O_2)W_4O_{14}$ adopt the same oxo-frameworks, due to cations with different charge and size, the local coordination environments of the polyhedra are essentially different. In $Nd(U^{V}O_2)W_4O_{14}$, structural refinement reveals distinct crystallographic sites which are practically fully occupied by Nd(III) and uranium U(V), enabling accurate measurement of U–O bond lengths. In contrast, for other lanthanide (Ln) cations of $Ln(U^{V}O_2)W_4O_{14}$ series, uranium(V) and the respective lanthanide(III) ions occupy identical crystallographic positions. These sites exhibit a partial occupancy, with a 50/50 distribution between U and Ln ions. Speculatively, that could be an effect of Ln-contraction where the smaller Ln-ions (up to 8% drop compared to Nd(III) radius) fit more to the local environment of U(V) and form the fully disordered structure. The most prominent dissimilarity is seen between UO_7 bipyramids. In structure of $Ca(U^{VI}O_2)W_4O_{14}$, the UO_7 pentagonal bipyramids have the average U=O bond distance 1.77(1) Å, and the average U–O bond distance for the equatorial oxygen is 2.35(1) Å. In case of $Ln(U^{V}O_2)W_4O_{14}$, however, the larger size of aliovalent dopants (Ln^{3+}) between neighbouring tungsten slabs $[W_4O_{11}]^{2+}$ create significantly bigger cavity volume which is no longer compatible with the geometry of hexavalent uranyl.

Consequently, the UO_7 pentagonal bipyramids in these cavities are forced to elongate their bond distances to fit the geometric restriction. For example, in Nd-based $Nd(U^{V}O_2)W_4O_{14}$, the U=O and equatorial U–O bond distances are 1.904(9) Å and 2.409(8) Å, respectively. Such elongations effectively result in a charge reduction of the uranium site, which is indicated by the result of bond valence calculation of 5.21 v.u.[26] Therefore, the polyhedral geometry and bond valence sum show that the lanthanide incorporation approach can lead to a dramatic elongation of uranium bonds needed for stabilizing pentavalent uranium. Thus, based on the crystallographic data we are able to propose a rare U(V) stabilization in the studied structures with Ln(III). To confirm that, we performed several different spectroscopic studies including X-ray absorption near edge structure in high energy resolution mode, X-ray photoelectron (XPS) and UV-Vis-NIR spectroscopies.

The U M_4-edge XANES measured in high-energy resolution fluorescence mode (details in Experimental and Theoretical

Methods) spectrum of $Nd(U^{V}O_2)W_4O_{14}$ is compared with the spectra of two reference compounds, UO_2 and $(U^{VI}O_2)Mo_2O_7 \bullet 3H_2O$ (mineral iriginite), in Figure 2. Iriginite and UO_2 contain U^{VI} forming uranyl type of bonding with two O axial (O_{ax}) atoms and U^{IV}, respectively.

The spectrum of iriginite exhibits three dominant peaks at about 3726.5 eV (A), 3728.7 eV (B) and 3732.7 eV (C). These spectral features have been described as transitions of $3d_{3/2}$ electrons to into 5fϕ/5fδ (A), 5fπ* (B) and 5fσ* (C) unoccupied valence orbitals of the uranyl molecule.[13] The energy position of the main peak A is clearly shifted with about -0.7 ± 0.05 eV to lower energies for the $Nd(U^{V}O_2)W_4O_{14}$ compound compared to the spectrum of iriginite. In addition, the energy shifts between the A and B (A–B), and A and C (A–C) peaks have noticeable reduction (A–B ≈ -0.8 eV, A–C ≈ -2 eV). These experimental results strongly suggest better screening of the $3d_{3/2}$ core-hole due to additional electron density on the U atom hence confirm the oxidation state V of U in $Nd(U^{V}O_2)W_4O_{14}$.

The spectrum of $Nd(U^{V}O_2)W_4O_{14}$ lies at about 1.6 ± 0.05 eV higher energies compared to the spectrum of UO_2; in addition, there are no features characteristic for U^{IV} present in the spectrum.[14,27,28] The hybridized U 5*f* and 6*p* orbitals form sigma bonds mainly with 2*p* orbitals of the O_{ax} atoms (5fσ* orbital)[29] therefore the energy position of peak C is strongly influenced by variations of the U=O_{ax} bond.[13] The reduced A–C distance for $Nd(U^{V}O_2)W_4O_{14}$ compared to iriginite is also an evidence for elongation of the U=O axial bond length in comparison to $Ca(U^{VI}O_2)W_4O_{14}$ in agreement with the XRD results.

To analyse the differences in the U M_4-edge XANES spectral profiles of the three $Ln(U^{V}O_2)W_4O_{14}$ compounds, with Ln = Nd, Sm and Gd, ligand-field density-functional theory (LFDFT) calculations were carried out. The model is based on atomic configuration interaction calculation, including the multiplet structures of U^{5+} $5f^1$ and $3d^95f^2$ electron configurations, and the oscillator strengths of the $5f^1 -> 3d^95f^2$ electron transitions. Ligand-field effect is also included by taking into account molecular cluster models that mimic the coordination sphere by the U^{5+} ion centre within the specific compounds. Figure 3

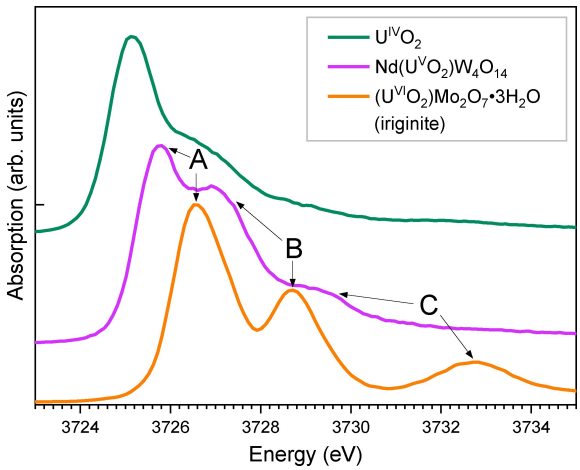

Figure 2. U M_4-edge XANES spectra of UO_2, $Nd(U^{V}O_2)W_4O_{14}$ and $(U^{VI}O_2)Mo_2O_7 \bullet 3H_2O$ (iriginte).

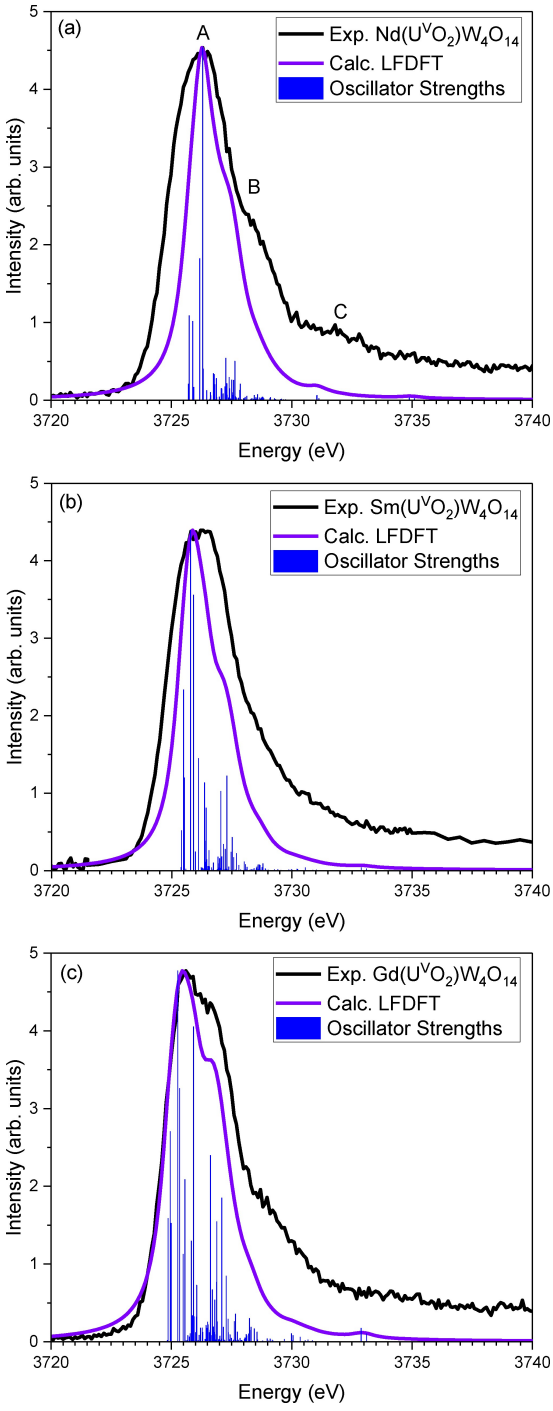

Figure 3. Comparison of the experimental spectra (Exp.) and the LFDFT calculation (Calc.) for the U M_4-edge XANES for (a) $Nd(U^{V}O_2)W_4O_{14}$, (b) $Sm(U^{V}O_2)W_4O_{14}$ and (c) $Gd(U^{V}O_2)W_4O_{14}$.

shows that the calculated spectra are in good agreement with the experimental data. The spectra are predominantly characterized by the ligand-field splitting of the U 5f orbitals, i.e., 5fϕ/5fδ (non-bonding orbitals), 5fπ* and 5fσ* (anti-bonding orbitals). Note that we use notation for cylindrical symmetry for the orbital representations for consistency with previous work.[13] The ground-state electronic structure is defined by 1 electron occupying the non-bonding orbitals. The observed spectra

shows electron transitions to the $3d^9 5f^2$ electron configuration. The main difference between the calculated spectra is in the energy shifts between the A–B and A–C peaks, which are smaller for the compound containing Nd and slightly increase and are similar for compounds with Sm or Gd. This indicates differential covalency effect of the U–O interaction, slightly larger bond covalency for the compounds with Gd and Sm, as shown previously.[13h] This trend is not that clear in the experimental data and further studies are necessary to describe the spectral trends. Note that the U M_4-edge XANES experimental spectra depicted in Figure 3 were recorded for powder samples, whereas the spectrum in Figure 2 was measured for a single crystal. Likely due to structural disorder and variations in the U-Oax bond for the compound with Nd, there are differences between the powder and the single crystal spectra. In addition, the spectra in Figure 3 are measured with lower experimental resulotion leading to learger spectral broadening. The differences in the spectra in Figures 2 and 3 do not affect the results of our study. It is also important to consider that the LFDFT calculations include the core-hole effect on the spectrum in the intermediate state (3d core-hole) but not in the final state (4f core-hole) of the U M_4-edge XANES spectra recorded in high-resolution mode. This can lead to differences between experiment and theory.

The U 4f XPS spectrum of $Nd(U^{V}O_2)W_4O_{14}$ (Figure 4) is charge referenced to carbon 1 s elemental line of adventitious hydrocarbon at 284.8 eV binding energy (BE), thus W $4f_{7/2}$ at 35.4 eV and O 1s at 530.4 eV. The U 4*f* doublet is fitted with two components and satellites characteristic for U^{5+} at a distance of about 8.7 eV to the 4*f* main lines.[30] The binding energy of the $4f_{7/2}$ main line at 380.1 eV (FWHM 1.3 eV) is in good agreement with values established for U^{5+} in KUO_3 and $Ba_2U_2O_7$.[31] The low binding energy of U $4f_{7/2}$, similar to UO_2, indicates enhanced electron density at uranium site. The presence of U^{6+} BEs peaks which also correspond to known values (381.5 eV for $4f_{7/2}$) is apparently the result of surface oxidation of U^{5+}.

The optical absorption spectra of $Ln(U^{V}O_2)W_4O_{14}$ were collected from the single crystals of all obtained members of the series including Nd, Sm, Gd, Eu and Yb countercations. As depicted in Figure 5, the spectra exhibit distinctive *f-f* electronic transitions characteristic of the aforementioned rare-earth elements.

This observation provides compelling evidence for the incorporation of the rare-earth cations into the crystal structures of these compounds. Additionally, a pronounced absorption feature, centered at approximately 550 nm, is observed. This feature is indicative of a charge-transfer band corresponding to the uranium (V) ion, signifying the presence of U(V) in these structures.[32] The spectral characteristics thus affirm the successful synthesis of $Ln(U^{V}O_2)W_4O_{14}$ compounds with the specified rare-earth countercations, shedding light on vital aspects of their electronic structure.

The preparation of alkaline-earth-based $Ca(U^{VI}O_2)W_4O_{14}$ and lanthanide-based $Ln(U^{V}O_2)W_4O_{14}$ by adopting different starting reagents exhibits a rare example of complete aliovalent substitution of considerably different cations while keeping the overall structural topology. This shows that the $M(UO_2)W_4O_{14}$ (M = alkaline- or rare-earth) is a potential matrix with unusual structural stability which tolerates considerable modification in composition without structural alteration. It can be envisioned that the incorporation of cations with varying charges into $M(UO_2)W_4O_{14}$ (M = alkaline- or rare-earth) necessitates electron transfer from the U–W–O anionic framework to achieve overall charge neutrality. Indeed, in the realm of defect chemistry, numerous charge conversion mechanisms have been postulated, particularly in materials like lanthanide-doped perovskite ($BaTiO_3$) or fluoride (CaF_2) ceramics.[33–36] However, a thorough understanding of the specific charge transfer mechanisms, including identifying exact lattice sites prone to cation substitution and the methodologies for achieving charge balance, remains elusive. This lack of clarity can be largely attributed to the dearth of definitive single crystal data, hindering the harmonization of theoretical and experimental insights in this field.[37,38] Actually, by analytically comparing the structural nuances of $Ca(U^{VI}O_2)W_4O_{14}$ and $Ln(U^{V}O_2)W_4O_{14}$, we are able to propose a viable charge-compensation mechanism. The result, shown in Figure 1 (c, d), demonstrates that when Ln^{3+} ions are introduced into the crystal structure, substituting for Ca^{2+} sites

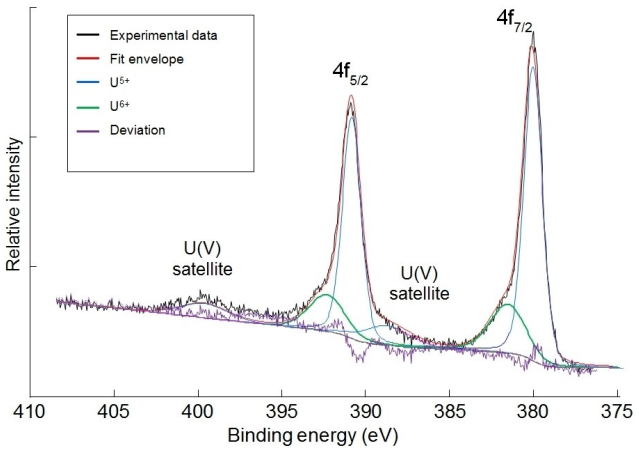

Figure 4. the U 4*f* XPS spectrum of $Nd(U^{V}O_2)W_4O_{14}$ with two components and the satellites for U^{5+}.

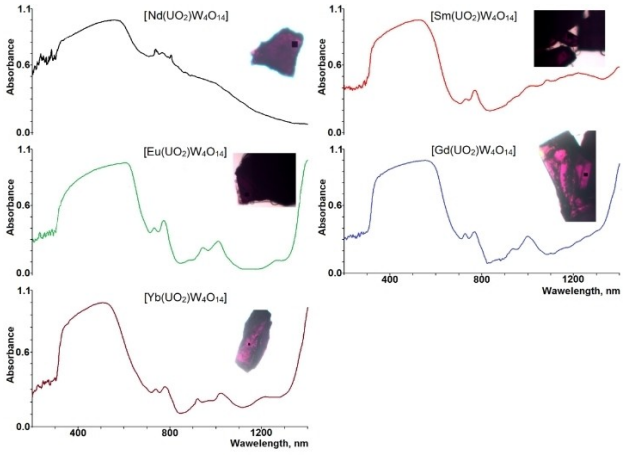

Figure 5. UV-vis-NIR absorption spectra and photographs of $Ln(U^{V}O_2)W_4O_{14}$ (Ln = Nd, Sm, Eu, Gd, and Yb).

and thereby introducing additional positive charge. This leads to a charge imbalance, which in turn triggers the reduction of uranium from U(VI) to U(V), with uranium acting as the electron acceptor. The dynamics of this charge transfer, initiated by the substitution process, are diagrammatically illustrated as follows:

$$Ca^{2+} = Ln^{3+} + e^{-} \quad (1)$$

$$e^{-} + U^{6+} = U^{5+} \quad (2)$$

Conclusions

In summary, by synthesizing the isostructural compound series $Ca(U^{VI}O_2)W_4O_{14}$ and $Ln(U^{V}O_2)W_4O_{14}$ (Ln = Nd, Sm, Eu, Gd, and Yb), this research successfully demonstrates the stabilization of hexavalent and pentavalent uranium within an alkaline-metal-based and a lanthanide-based oxo-framework, respectively. Notably, $Ln(U^{V}O_2)W_4O_{14}$ is the first structurally characterized material combining pentavalent uranium with rare-earth metals, exhibiting a novel U–Ln cation-cation interaction. Our results showed that aliovalent substitution of Ca^{2+} by Ln^{3+} in the iriginite-related structures provides an effective way to build novel heterometallic *5f–4f* cation-cation interaction assemblies. It is also a highly facile and reproducible route to stabilize pentavalent uranium.

The compounds were extensively characterized by means of single crystal X-ray diffraction as well U M_4-edge XANES, XPS and UV-Vis-NIR spectroscopy. The research revealed that the charge differences introduced into the oxo-framework by the inclusion of Ca^{2+} or Ln^{3+} ions are effectively neutralized by adjusting the local structural configuration. This adjustment leads to a change in the uranium oxidation states from U(VI) to U(V). Furthermore, this study suggests the feasibility of preparing charge-tunable $Ca_xLn_{1-x}(U^{VI}_yU^{V}_{1-y}O_2)W_4O_{14}$ complexes by modifying the Ca^{2+}/Ln^{3+} ratio. This possibility raises questions about the potential electronic, bonding, structural, and magnetic properties of such complexes. The structural and charge tunability of the uranyl units hints at a wide range of applications, necessitating further research to explore these aspects.

Experimental and Theoretical Method

Crystal Growth and SCXRD of $Ln(U^{V}O_2)W_4O_{14}$ Series

The compounds discussed in this work were obtained by high-temperature solid state reactions from mixtures of $UO_2(NO_3)_2{\cdot}6H_2O$, WO_3 and $Ln(NO_3)_3{\cdot}xH_2O$ (Ln = Nd, Sm, Gd, Eu or Yb, x = 5 or 6) with molar ratio U:W:Ln = 1:4:1 (initial mass of uranyl nitrate −0.1 g). These mixtures were heated to 1200 °C in platinum crucibles for 4 h and cooled down to 400 °C with the rate of 7 °C h^{-1}. The reaction yielded the mixture of dark-red ($Ln(U^{V}O_2)W_4O_{14}$), green (WO_3), yellow (uranium tungstate). For Nd synthesis, dark brown crystals ($Nd_{14}W_{22}O_{44}$) were also found. Dark-red blocks of $Ln(U^{V}O_2)W_4O_{14}$ suitable for single-crystal XRD were manually separated from side products. EDS analysis shows the ratio of Ln: U = 1: 1 in all the obtained crystals. For single crystal X-ray diffraction experiments was used an Agilent SuperNova (Dual Source) diffractometer. The crystal data were collected by means of monochromatic Mo-Kα (0.71073 Å), equipped with micro-focus X-ray tube technology, running at 50 kV and 0.8 mA, providing a beam size of approximately 30 μm. Standard CrysAlisPro software was used for calculating the dimensions of the unit cells as well as for controlling data collections. More than a hemisphere of data was collected for each crystal. After collection, data were corrected for Lorentz, polarization, absorption and background effects.

U M_4-Edge XANES Spectroscopy

The U M_4-edge (3728 eV) high-energy resolution XANES experiments (usually named as HERFD- or HR-XANES) were performed at the ID26 beamline at the European Synchrotron Radiation Facility (ESRF), Grenoble, France (spectra in Figure 2) and at the ACT station of the CAT-ACT beamline at the KIT Light Source, Karlsruhe Institute of Technology, Karlsruhe, Germany (spectra in Figure 3).[39,40, 41] The incident energy was monochromatized by a Si(111) double crystal monochromator (DCM). Rejection of higher harmonics was achieved by three Si mirrors at an angle of 3.5 mrad (ID26). The beam size was focused to ≈ 0.150 mmn (ID26)/0.5 mm (ACT) vertical and ≈ 0.450 mm (ID26)/0.5 mm (ACT) horizontal dimensions for the measurements at U M_4-edge XANES spectra were measured in high-energy resolution detection mode using an X-ray emission spectrometer.[41] The sample, analyzer crystal and silicon drift diode detector (SDD) (ID26)/(Ketek, a single element solid state detector) (ACT) were arranged in a vertical Rowland geometry. The paths of the incident and emitted X-rays through air were minimized in order to avoid losses in intensity due to absorption. The U high energy resolution XANES spectra at the M_4-edge were obtained by recording the maximum intensity of the M_β emission line (U M_β = 3337 eV) with five spherically bent Si(220) crystal analyzers with 1 m bending radius. The crystals were aligned at 75° Bragg angle. The experimental energy resolution was 0.7 eV at ID26 determined by measuring the full width at half maximum (FWHM) of the elastic peak. Samples were confined by thin layer of Kapton (with 25microns thickness). The experimental energy resolution is estimates to be about 1 eV at ACT. Measurements have been performed at the room temperature conditions. At ID26, 15 scans with 10 sec measuring time per scan were collected and averaged for one $Nd(U^{V}O_2)W_4O_{14}$ crystal with size of about 100 x 100 μm^2. No changes of the spectra caused by radiation damage were observed. The crystal was preliminary measured with attenuator (Al foil with 200 μm thickness) for 5 seconds. The spectra measured with and without Al foil differ only by the signal to noise ratio. Seven additional $Nd(U^{V}O_2)W_4O_{14}$ crystals with similar sizes were also measured. The spectral features marked A, B and C in Figure 2 have strong intensity variations (not shown here) likely caused by different orientations of the polarization vector of the incident X-ray beam with respect to the O=U=O axis of uranyl. No substantial energy shifts of the peaks were detected. The uranyl unites are parallel to each other in the $Nd(U^{V}O_2)W_4O_{14}$ crystals, which however were randomly oriented with respect to each other during the measurements. For the spectrum shown in Figure 2 the O=U=O axis has close to 90° orientation with respect to ε since the A peak has significantly higher intensity than B peak.[27] Powder $Ln(U^{V}O_2)W_4O_{14}$ (Ln=Nd, Sm or Gd) compounds were mixed with boron nitride and pellets with 7 mm diameter were pressed and measured at ACT to obtain the spectra in Figure 3.

U 4f XPS

X-ray Photoelectron Spectroscopy (XPS) was performed by a system PHI 5000 VersaProbe II (ULVAC-PHI Inc.) equipped with a scanning microprobe X-ray source (monochromatic Al Kα (1486.7 eV) X-rays).

Low energy electrons (1 eV) and low energy argon ions (8 eV) were applied simultaneously for charge compensation at isolating sample surface (dual beam technique). Calibration of the binding energy scale of the spectrometer was performed using well-established binding energies of elemental lines of pure metals (surface cleaned by Ar ion beam sputtering (3 keV), monochromatic Al Kα: Cu $2p_{3/2}$ at 932.62 eV, Au $4f_{7/2}$ at 83.96 eV).[42] Standard deviations of binding energies of isolating samples were within ±0.2 eV. Crystals were pressed onto an indium foil and mounted onto the sample holder. The base pressure inside the spectrometer was about 2×10^{-7} Pa. To retrieve information about the chemical state of the elements, narrow scan spectra of elemental lines were recorded at a pass energy of 23.5 eV of the analyzer. Spectra were charge referenced to C 1s elemental line of adventitious hydrocarbon at 284.8 eV. Curve fits to elemental lines were performed by a non-linear least-squares optimization procedure using Gaussian–Lorentzian sum functions after Shirley background subtraction by PHI MultiPak Version 9.6 data analysis program.

UV-Vis-NIR and Photoluminescence

UV-vis-NIR and photoluminescence data were acquired from single crystals using a Craic Technologies microspectrophotometer. Crystals were placed on quartz slides under Krytox oil, and the data were collected from 200 to 1,400 nm. The exposure time was auto optimized by the Craic software. Photoluminescence data were acquired using the same microspectrophotometer with an excitation wavelength of 365 or 420 nm. Temperature control was achieved by using a Linkam temperature control stage.

LFDFT Calculations

The U M_4-edge XAS spectra were calculated using the ligand-field density-functional theory (LFDFT) method.[43–44] All calculations were done by using the hybrid Perdew-Burke-Ernzerhof PBE0 functional.[45] Molecular orbitals were expanded by means of the all-electron Slater-type orbitals basis set of quadrupole-zeta augmented by four sets of polarization function (QZ4P) for all elements. Relativistic corrections were included by using the zeroth-order regular approximation (ZORA) of the Dirac equation method at the scalar and spin-orbit levels of theory. The starting atomic inputs were based on the experimental crystallographic structures of the $Ln(U^{V}O_2)W_4O_{14}$ compounds by using molecular cluster models. For $Nd(U^{V}O_2)W_4O_{14}$, the molecular cluster model consisted of the $[UO_2O_6]^{11-}$ moiety plus two $[NdO]^{1+}$ units directly interacting with the two uranyl oxo-groups. For $Sm(U^{V}O_2)W_4O_{14}$ and $Gd(U^{V}O_2)W_4O_{14}$, the same molecular cluster models included the $[UO_2O_5]^{9-}$ moiety plus two $[LnO]^{1+}$ units. Point-charges were added to mimic the long-range interaction and the periodicity of the crystal structures. This point charges included the positions of the neighboring W, O, U and Ln atoms of the molecular cluster models. Note that LFDFT allowed calculation of the U M4-edge XAS spectra based on multiplet structures and the oscillator strengths of the actinide $5f^1 -> 3d^95f^2$ electron transitions at the density-functional theory (DFT) level of theory. The calculation procedure can be found elsewhere.[46] It has been shown that LFDFT is very well suited to deal with actinide coordination compounds,[47–48] and x-ray spectroscopy in particular. Briefly, an effective Hamiltonian was defined to calculate multi-electronic problems with $5f^1$ and $3d^95f^2$ electron configurations that represented the ground (GS) and final (FS) states of the U M4-edge XAS process. For that, we started with DFT calculations where we forced partial electron occupation on selective molecular orbitals with large fractional parentage coefficients for U functions. This was an average of configuration (AOC) DFT-type calculation, where open-shell electrons are evenly distributed over near-degenerate molecular orbitals to obtain a totally symmetric electron density that was isomorphic with the ligand-field effective Hamiltonian. This could be achieved by using the keyword "IrrepOccupations" in ADF. Note that the presence of the two lanthanide ions in the molecular cluster models induced additional challenges in the electronic structure. To simplify the calculation, we froze the lanthanide 4f electrons in both GS and FS electronic structures, i.e. they were also evenly distributed in the 14 molecular orbitals that were formally identified with large fractional parentage coefficients for Ln 4f. These orbitals were excluded in the LFDFT calculations. For GS ($5f^1$), the sevenfold molecular orbitals that were identified with large fractional parentage coefficients for U 5f are occupied with 0.1429 electron. For FS ($3d^95f^2$), the same sevenfold molecular orbitals were occupied with 0.2857 electrons, as we removed 1 electron from the core U 3d orbitals (i.e. the fivefold U 3d based molecular orbitals were occupied with 1.8 electron). Supplementary Figure S6 shows the calculated density of states (DOS) as function of GS and FS electronic structures for the three $Ln(U^{V}O_2)W_4O_{14}$ compounds. Figure S6 also shows the changes in the U 5f DOS from GS to FS, overall shifting of the U 5f molecular orbitals to lower energy as screening of the U 3d core-hole. Ligand-field parameters were calculated based on the GS and FS electronic structures. These parameters included the Slater-Condon integrals F^k(5f,n5f), with k = 0, 2, 4, 6, F^k(3d, 5f), with k = 0, 2, 4 and G^k(3d, 5f), with k = 1, 3, 5; the spin-orbit coupling constants ζ_{3d} and ζ_{5f}; and the 5×5 and 7×7 matrices that represented the 3d and 5f ligand-field potential.

Acknowledgements

Authors are very grateful to Prof. Kristina Kvashnina (ESRF/HZDR) for her help in the synchrotron data collection. EVA, is grateful for DFG for the funding within AL1527/3-1 project. YY is supported with the National Natural Science Foundation of China (12264004), the Natural Science Foundation of Jiangxi Province (20202ACBL214020). YH are supported by Natural Science Foundation of Anhui Province (2008085QB56), Hefei University New Era Education Quality Project (2021Yyykc02) and Anhui New Era Education Quality Project for Graduate (2022qyw/sysfkc042). ESRF is acknowledged for providing the beamtime at ID26 beamline. Help from Patrick Colomp and ESRF safety group in handling uranium compounds at the beamline is greatly acknowledged. T. V. and H. R. acknowledge financial support from the Deutsche Forschungsgemeinschaft (DFG, German Research Foundation) through the Collaborative Research Centre "4f for Future" project A1 (CRC 1573, project number 471424360) and the European Research Council (ERC) Consolidator Grant 2020 under the European Union's Horizon 2020 research and innovation program (grant agreement no. 101003292). We thank the Institute for Beam Physics and Technology (IBPT) for the operation of the storage ring, the Karlsruhe Research Accelerator (KARA). We thank the KIT Light Source for provision of beamtime. Open Access funding enabled and organized by Projekt DEAL.

Conflict of Interests

The authors declare no conflict of interest.

Data Availability Statement

The data that support the findings of this study are available in the supplementary material of this article.

Keywords: Actinides · Uranium · Pentavalent uranyl complexes · Iriginite · Oxo-salt

[1] a) S. K. Cary, M. Vasiliu, R. E. Baumbach, J. T. Stritzinger, T. D. Green, K. Diefenbach, J. N. Cross, K. L. Knappenberger, G. Liu, M. A. Silver, A. E. DePrince, M. J. Polinski, S. M. Van Cleve, J. H. House, N. Kikugawa, A. Gallagher, A. A. Arico, D. A. Dixon, T. E. Albrecht-Schmitt, *Nat. Commun.* **2015**, *6*, 6827; b) Y. Hao, G. L. Murphy, D. Bosbach, G. Modolo, T. E. Albrecht-Schmitt, E. V. Alekseev, *Inorg. Chem.* **2017**, *56*, 9311; c) Y. Hao, V. V. Klepov, G. L. Murphy, G. Modolo, D. Bosbach, T. E. Albrecht-Schmitt, B. J. Kennedy, S. Wang, E. V. Alekseev, *Cryst. Growth Des.* **2016**, *16*, 5923.

[2] a) B. Xiao, T. M. Gesing, L. Robben, D. Bosbach, E. V. Alekseev, *Chem. Eur. J.* **2015**, *21*, 7629; b) Y. Hao, V. V. Klepov, P. Kegler, G. Modolo, D. Bosbach, T. E. Albrecht-Schmitt, S. Wang, E. V. Alekseev, *Cryst. Growth Des.* **2018**, *18*, 498; c) Y. Hao, P. Kegler, D. Bosbach, T. E. Albrecht-Schmitt, S. Wang, E. V. Alekseev, *Cryst. Growth Des.* **2017**, *17*, 5898; .

[3] a) B. Xiao, M. Klinkenberg, D. Bosbach, E. V. Suleimanov, E. V. Alekseev, *Inorg. Chem.* **2015**, *54*, 5981; b) Y. Hao, P. Kegler, T. E. Albrecht-Schmitt, S. Wang, Q. Dong, E. V. Alekseev, *Eur. J. Inorg. Chem.* **2020**, *4*, 407.

[4] a) F. Burdet, J. Pécaut, M. Mazzanti, *J. Am. Chem. Soc.* **2006**, *128*, 16512; b) Y. Hao, G. L. Murphy, P. Kegler, Y. Li, P. M. Kowalski, S. Blouin, Y. Zhang, S. Wang, L. Robben, T. M. Gesing, E. V. Alekseev, *Dalton Trans.* **2022**, *51*, 13376; c) Y. Hao, E. V. Alekseev, V. V. Klepov, N. Yu, *Eur. J. Inorg. Chem.* **2020**, *33*, 3187.

[5] a) L. Barluzzi, F. C. Hsueh, R. Scopelliti, B. E. Atkinson, N. Kaltsoyannis, M. Mazzanti, *Chem. Sci.* **2021**, *12*, 8096; b) Z. Z. Pan, B. Bártová, T. L. Grange, S. M. Butorin, N. C. Hyatt, M. C. Stennett, K. O. Kvashnina, R. B. Latmani, *Nat. Commun.* **2020**, *11*, 4001.

[6] a) P. Rungthanaphatsophon, K. S. Welsh, R. J. Ward, S. P. Kelley, W. W. Lukens, A. Kerridge, J. R. Walensky, *Organometallics* **2023**, *42*, 1404; b) M. X. Zhang, C. Y. Liang, G. D. Cheng, J. C. Chen, Y. M. Wang, L. W. He, L. W. Cheng, S. C. Gong, D. Zhang, J. Li, S. X. Hu, J. D. Wu, G. Z. Wu, Y. X. Wang, Z. F. Chai, S. A. Wang, *Angew. Chem. Int. Ed.* **2021**, *60*, 9886.

[7] a) M. R. MacDonald, M. E. Fieser, J. E. Bates, J. W. Ziller, F. Furche, W. J. Evans, *J. Am. Chem. Soc.* **2013**, *135*, 13310; b) Y. Hao, E. M. Langer, B, Xiao, P. Kegler, X. Cao, K. Hu, R.-A. Eichel, S. Wang, E. V. Alekseev, *Front. Chem.* **2023**, *11*, 1152113.

[8] T. A. Sullens, R. A. Jensen, T. Y. Shvareva, T. E. Albrecht-Schmitt, *J. Am. Chem. Soc.* **2004**, *126*, 2676.

[9] a) G. E. Jamal, T. Gouder, R. Eloirdi, M. Jonsson, *Dalton Trans.* **2021**, *50*, 729; b) K. Yuan, M. R. Antonio, E. S. Ilton, Z. R. Li, U. Becker, *ACS Earth Space Chem.* **2022**, *6*, 1024.

[10] P. Rungthanaphatsophon, K. Stanistreet-Welsh, R. J. Ward, S. P. Kelley, W. W. Lukens, A. Kerridge, J. R. Walensky, *Organometallics* **2023**, *42*, 1404.

[11] a) R. Faizova, F. F. Tirani, R. B. Latmani, M. Mazzanti, *Angew. Chem.* **2020**, *132*, 6822; b) X. Q. Xin, I. Douair, T. Rajeshkumar, Y. Zhao, S. A. Wang, L. Maron, C. Q. Zhu, *Nat. Commun.* **2022**, *13*, 3809.

[12] D. X. Gu, W. T. Yang, H. P. Chen, Y. H. Yang, X. D. Qin, L. Chen, S. Wang, Q. H. Pan, *Inorg. Chem. Front.* **2021**, *8*, 3514.

[13] a) T. Vitova, I. Pidchenko, D. Fellhauer, P. Bagus, Y. Joly, T. Pruessmann, S. Bahl, E. Gonzalez-Robles, J. Rothe, M. Altmaier, M. Denecke, H. Geckeis, *Nat. Commun.* **2017**, *8* (1), 16053; b) L. Amidani, M. Retegan, A. Volkova, K. Popa, P. M. Martin, K. O. Kvashnina, *Inorg. Chem.* **2021**, *60* (21), 16286–16293; c) K. O. Kvashnina, S. M. Butorin, *Chem. Commun.* **2022**, *58*, 327–342; d) J. N. Ehrman, K. Shumilov, A. J Jenkins, J. M Kasper, T. Vitova, E. R Batista, P. Yang, X. Li, *JACS Au.* **2024**, *4*, 1134–1141; e) R. Polly, B. Schacherl, J. Rothe, T. Vitova, *Inorg. Chem.* **2021**, *60* (24), 18764–18776; f) T. Vitova, I. Pidchenko, S. Biswas, G. Beridze, P. W. Dunne, D. Schild, Z. Wang, P. M. Kowalski, R. J. Baker, *Inorg. Chem.* **2018**, *57* (4), 1735–1743; g) Y. Podkovyrina, I. Pidchenko, T. Prüßmann, S. Bahl, J. Göttlicher, A. Soldatov, T. Vitova, *J. Phys.: Conf. Ser.* **2016**, *712*, 012092; h) M. Zegke, X. Zhang, I. Pidchenko, J. A. Hlina, R. M. Lord, J. Purkis, G. S. Nichol, N. Magnani, G. Schreckenbach, T. Vitova, J. B. Love, P. L. Arnold, *Chem. Sci.* **2019**, *10*, 9740.

[14] I. Pidchenko, K. Kvashnina, T. Yokosawa, N. Finck, S. Bahl, D. Schild, R. Polly, E. Bohnert, A. Rossberg, J. Göttlicher, K. Dardenne, J. Rothe, T. Schäfer, H. Geckeis, T. Vitova, *Environ. Sci. Technol.* **2017**, *51* (4), 2217–2225.

[15] Z. Yang, C. X. Wang, D. Q. Liu, Y. L. Li, Y. Ning, S. Yang, Y. Y. Zhang, Y. Tang, Z. Tang, W. Zhang, *J. Cleaner Prod.* **2019**, *233*, 115.

[16] Z. Z. Pan, Y. Roebbert, A. Beck, B. Bartova, T. Vitova, S. Weyer, R. Bernier-Latmani, *Environ. Sci. Technol.* **2022**, *56*, 1753.

[17] M. X. Zhang, C. Y. Liang, G. D. Cheng, J. C. Chen, Y. M. Wang, L. W. He, L. W. Cheng, S. C. Gong, D. Zhang, J. Li, S. X. Hu, J. D. Wu, G. Z. Wu, Y. X. Wang, Z. F. Chai, S. A. Wang, *Angew. Chem. Int. Ed.* **2021**, *60*, 9886.

[18] L. T. Townsend, K. Morris, R. Harrison, B. Schacherl, T. Vitova, L. Kovarik, C. I. Pearce, J. F. W. Mosselmans, S. Shaw, *Chemosphere* **2021**, *276*, 130117.

[19] S. J. Li, Y. Z. Hu, Z. W. Shen, Y. W. Cai, Z. Y. Ji, X. L. Tan, Z. X. Liu, G. X. Zhao, S. X. Hu, X. K. Wang, *Sci. China Chem.* **2021**, *64*, 1323.

[20] a) K. Ouchi, D. Matsumura, T. Tsuji, T. Kobayashi, H. Otobe, Y. Kitatsuji, *RSC Adv.* **2023**, *13*, 16321; b) G. Leinders, R. Bes, K. O. Kvashnina, M. Verwerft, *Inorg. Chem.* **2020**, *59*, 4576; c) X. L. Liu, Y. H. Xie, M. J. Hao, Z. S. Chen, H. Yang, G. l. N. Waterhouse, S. Q. Ma, X. K. Wang, *Adv. Sci.* **2022**, *9*, 2201735.

[21] N. Jori, L. Barluzzi, I. Douair, L. Maron, F. Fadaei-Tirani, I. Z|uivković, M. Mazzanti, *J. Am. Chem. Soc.* **2021**, *143*, 11225.

[22] V. Serezhkin, V. Efremov, V. Trunov, *Geokhimiya* **1981**, *13*, 451.

[23] S. V. Krivovichev, P. C. Burns, *Solid State Sci.* **2003**, *5*, 373.

[24] S. V. Krivovichev, P. C. Burns, *Can. Mineral.* **2000**, *38*, 847.

[25] S. V. Krivovichev, P. C. Burns, *Can. Mineral.* **2002**, *40*, 1571.

[26] P. C. Burns, R. C. Ewing, F. C. Hawthorne, *Can. Mineral.* **1997**, *35*, 1551.

[27] T. Vitova, J. C. Green, R. G. Denning, M. Loble, K. Kvashnina, J. J. Kas, K. Jorissen, J. J. Rehr, T. Malcherek, M. A. Denecke, *Inorg. Chem.* **2015**, *54*, 174.

[28] K. O. Kvashnina, S. M. Butorin, P. Martin, P. Glatzel, *Phys. Rev. Lett.* **2013**, *111*, 253002.

[29] R. G. Denning, *J. Phys. Chem. A* **2007**, *111*, 4125.

[30] a) E. S. Ilton, P. S. Bagus, *Surf. Interface Anal.* **2011**, *43*, 1549; b) D. X. Gu, W. T. Yang, H. P. Chen, Y. H. Yang, X. D. Qin, L. Chen, S. Wang, Q. H. Pan, *Inorg. Chem. Front.* **2021**, *8*, 3514.

[31] J. H. Liu, S. Van den Berghe, M. J. Konstantinović, *J. Solid State Chem.* **2009**, *182*, 1105.

[32] J. T. Stritzinger, E. V. Alekseev, M. J. Polinski, J. N. Cross, T. M. Eaton, T. E. Albrecht-Schmitt, *Inorg. Chem.* **2014**, *53*, 5294.

[33] C. L. Freeman, J. A. Dawson, H. R. Chen, J. H. Harding, L. B. Ben, D. C. Sinclair, *J. Mater. Chem.* **2011**, *21*, 4861.

[34] C. L. Freeman, J. A. Dawson, H. R. Chen, L. Ben, J. H. Harding, F. D. Morrison, D. C. Sinclair, A. R. West, *Adv. Funct. Mater.* **2013**, *23*, 3925.

[35] J. L. Merz, P. S. Pershan, *Phys. Rev.* **1967**, *162*, 217.

[36] M. Viviani, M. T. Buscaglia, V. Buscaglia, L. Mitoseriu, A. Testino, P. Nanni, D. Vladikova, *J. Eur. Ceram. Soc.* **2004**, *24*, 1221.

[37] F. Morrison, A. Coats, D. Sinclair, A. West, *J. Electroceram.* **2001**, *6*, 219.

[38] I. Akin, M. Li, Z. Lu, D. C. Sinclair, *RSC Adv.* **2014**, *4*, 32549.

[39] a) S. M. Butorin, K. O. Kvashnina, D. Prieur, M. Rivenet, P. M. Martin, *Chem. Commun.* **2017**, *53*, 115; b) A. Zimina, K. Dardenne, M. A. Denecke, D. E. Doronkin, E. Huttel, H. Lichtenberg, S. Mangold, T. Pruessmann, J. Rothe, Th. Spangenberg, R. Steininger, T. Vitova, H. Geckeis, J. D. Grunwaldt, *Rev. Sci. Instrum.* **2017**, 113113.

[40] B. Schacherl, T. Prüssmann, K. Dardenne, K. Hardock, V. Krepper, J. Rothe, T. Vitova, H. Geckeis, *J. Synchrotron Radiat.* **2022**, *6*, 164.

[41] Glatzel, et al, *J. Synchrotron Radiat.* **2021**, *29*(1), 80–88.

[42] M. P. Seah, I. S. Gilmore, G. Beamson, *Surf. Interface Anal.* **1998**, *26*, 642.

[43] H. Ramanantoanina, *Computation* **2022**, *10* (5), 70.

[44] ADF 2023.1, SCM, Theoretical Chemistry, Vrije Universiteit, Amsterdam, The Netherlands, http://www.scm.com.

[45] M. Ernzerhof, G. E. Scuseria, *J. Chem. Phys.* **1999**, *110*, 5029–5036.

[46] H. Ramanantoanina, *J. Chem. Phys.* **2018**, *149*, 054104.

[47] J. G. Tobin, et al, *J. Vac. Sci. Technol. A* **2023**, *41*, 063208.

[48] J. G. Tobin, et al, *Phys. Rev. B* 2002 105, 125129.

Manuscript received: March 13, 2024
Accepted manuscript online: May 22, 2024
Version of record online: June 28, 2024